



HAL
open science

Absolute and Relative Positioning of Natural Organic Matter Acid–Base Potentiometric Titration Curves: Implications for the Evaluation of the Density of Charged Reactive Sites

Marawit Tesfa, Jerome F.L. Duval, Remi Marsac, Aline Dia, José-Paulo F Pinheiro

► To cite this version:

Marawit Tesfa, Jerome F.L. Duval, Remi Marsac, Aline Dia, José-Paulo F Pinheiro. Absolute and Relative Positioning of Natural Organic Matter Acid–Base Potentiometric Titration Curves: Implications for the Evaluation of the Density of Charged Reactive Sites. *Environmental Science and Technology*, 2022, 56 (14), pp.10494-10503. 10.1021/acs.est.2c00828 . hal-03704908

HAL Id: hal-03704908

<https://hal.univ-lorraine.fr/hal-03704908>

Submitted on 26 Jun 2022

HAL is a multi-disciplinary open access archive for the deposit and dissemination of scientific research documents, whether they are published or not. The documents may come from teaching and research institutions in France or abroad, or from public or private research centers.

L'archive ouverte pluridisciplinaire **HAL**, est destinée au dépôt et à la diffusion de documents scientifiques de niveau recherche, publiés ou non, émanant des établissements d'enseignement et de recherche français ou étrangers, des laboratoires publics ou privés.

Absolute and relative positioning of natural organic matter acid-base potentiometric titration curves: implications for the evaluation of density of charged reactive sites

Marawit TESFA*¹, Jérôme F.L. DUVAL*², Rémi MARSAC¹, Aline DIA¹, Jose-Paulo PINHEIRO²

¹ Université Rennes, CNRS, Géosciences Rennes – UMR 6118, F-35000 Rennes, France

² Université de Lorraine, CNRS, LIEC (Laboratoire Interdisciplinaire des Environnements), UMR 7360 Continentaux, 54500 Vandoeuvre-Lès-Nancy, France

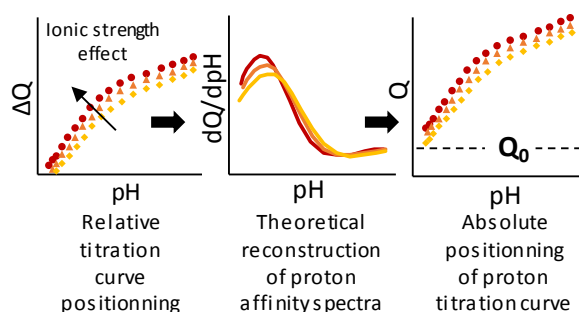
*Corresponding authors. [Marawit TESFA](mailto:marawit.tesfa@univ-rennes1.fr) (marawit.tesfa@univ-rennes1.fr), Jérôme F.L. DUVAL (jerome.duval@univ-lorraine.fr).

Abstract. Potentiometric acid-base titration curves collected on humic (nano)particles as a function of pH and salt concentration reflect the electrostatics of the particles and the amount of chemical charges (Q) they carry. In turn, interpretation of titration data helps quantifying their reactivity towards metals provided that both intrinsic chemical and non-specific electrostatic contributions to proton binding are correctly unraveled. Establishing a titration curve requires several steps, i.e. blank subtraction, relative curve positioning with respect to electrolyte concentration, and absolute curve positioning achieved by estimation of particle charge Q_0 at low pH. Failure in establishing properly each step may lead to misevaluation of nanoparticle charging behavior. Here, we report (i) a simple procedure to measure and position titration curves for humic substances (HS) versus salt concentration, and (ii) an original approach for absolute curve positioning upon exploitation of proton affinity spectra. The latter do not depend on Q_0 and they thus constrain titration data analysis using Soft Poisson Boltzmann-based Titration (SPBT) formalism for nanoparticles in the thick electric double layer regime. We illustrate the benefits of our approach by analyzing titration measurements for a large range of humic nanoparticles and by comparing the outcome with results from literature.

Synopsis. This article provides a simple and accurate approach to determine the acid-base properties and electrostatic features of humic nanoparticles.

Keywords: Humic substances, Proton titration curves, Potentiometry, Soft particle electrostatics, Nanoparticles.

Graphical abstract



Introduction

Natural Organic Matter (NOM) is ubiquitous in the environment and plays a paramount role in geochemical cycling of elements and in numerous biotic and abiotic chemical reactions.¹⁻³ NOM has a complex structure, humification state and composition depending on origin, operative hydro-biogeochemical conditions, types and biochemical activity of (micro)organisms that formed NOM by degradation processes. Consequently, NOM reactivity towards a diversity of compounds, including contaminants, remains difficult to understand and predict at a mechanistic level.

Reactions between NOM and protons or metallic contaminants (cations in general) are mainly driven by acid-base functional groups, including carboxylic groups and minor reactive sites such as phenolic groups (amongst sulfur, nitrogen or phosphorous functional groups).^{4,5} In this study as in many others related to humic reactivity, only carboxylic and phenolic groups will be considered because they represent the large majority of the proton binding sites. Humic substances (HS) can be divided into humic (HA) and fulvic acids (FA) on the basis of their respective solubility.⁶ They are key components of NOM as they carry the majority of carboxylic and phenolic groups. For this reason, the analysis of cation-HS binding processes has been the topic of numerous studies in literature (e.g.⁷⁻¹³). Since HS are chemically heterogeneous, a large variety of carboxylic- and phenolic-types of functional groups are found in contrasted chemical environments, and their respective reactivity involves differentiated chemical affinity towards cationic species. In addition, HS are colloids defined by nanometric dimensions, with radii of ca. 1 to 10 nm.¹⁴ They carry an electrical charge resulting from the formation of complexes between cations and reactive sites distributed throughout their intraparticulate volume. The assumption of equilibrium metal complexation by (nano)particulate ligands like HS, as formulated in the commonly adopted Biotic Ligand Model (BLM) and Free Ion Activity Model (FIAM), is tied to the verification of dynamic criteria,¹⁵⁻¹⁷

1
2
3 65 and for both scenarios of equilibrium and non-equilibrium metal speciation/complexation, the
4 66 estimation of metal (bio)availability in suspension containing (nano)particulate ligands like HS
5
6 67 requires proper evaluation of HS metal binding sites, metal binding heterogeneity and a proper
7
8 68 integration of the HS electric double layer properties.^{18–21} This is where proton titration method
9
10 69 comes in as this method allows for the determination of these properties.

11 70 Because cations and protons compete for the same binding groups, it is fundamental to
12 71 determine HS acid-base properties, which includes amounts and dissociation constants of
13 72 carboxylic and phenolic groups. For that purpose, acid-base potentiometric titration curves are
14 73 commonly collected as a function of pH and salt concentration, and subsequently analyzed by
15 74 thermodynamic modeling.^{22,23} The method consists in performing successive acid-base
16 75 titrations for a given HS sample dispersed in a monovalent background electrolyte (e.g. NaCl,
17 76 KNO₃), whose concentration is generally increased to achieve three ionic strengths (IS)
18 77 typically in the range 3 to 300 mM. The sample is first acidified to reach the lowest chosen pH
19 78 value ($3 \leq \text{pH} \leq 4$) at the lowest salt concentration adopted for the measurement. Then, the
20 79 sample is titrated with a base, up to the highest chosen pH (typically $10 \leq \text{pH} \leq 11$), followed
21 80 by an acid titration back to the original pH. These titrations are repeated to obtain replicates at
22 81 fixed salt concentration (forward and reverse measurements). To increase IS, salt is added at
23 82 the lowest pH and titration procedure is then iterated for the second and third IS condition
24 83 tested. The evaluation of the amount of H⁺ or OH⁻ consumed by HS provides a direct
25 84 quantification of the number of deprotonated groups as a function of pH over the whole HS
26 85 dispersion volume. This number can then be converted into a variation of the (negative)
27 86 electrical charge carried by HS (denoted as ΔQ) relative to the charge of the material at the
28 87 initial pH of the titration curve (denoted hereafter to as Q_0). Analysis of the dependence of HS
29 88 charge variation on pH and salt concentration further requires adequate estimation of the
30 89 chemical (intrinsic) and electrostatic (non-specific) contributions to the proton affinity for HS
31 90 carboxylic and phenolic groups, which requires modeling.^{17,19–24}

32
33
34
35
36
37
38
39
40
41
42
43
44
45 91 Despite of the apparent simplicity of the aforementioned proton titration procedure, major
46 92 experimental challenges must be addressed to achieve accurate determination of HS acid-base
47 93 properties. Two of them are listed below:

48
49
50 94 (i) A major difficulty concerns the estimation of the absolute charge (Q) of HS materials as
51 95 a function of pH. Even though the necessity to assess Q_0 value is recognized to compute
52 96 Q from ΔQ , there is, to the best of our knowledge, currently no clear method proposed to
53 97 evaluate Q_0 . In literature, the way Q_0 is estimated is either not described^{25–27} or tied to its
54 98 adjustment within multiparametric modeling-based fitting exercise.^{28,29} A possible way

1
2
3 99 to estimate Q_0 would consist in measuring the point of zero salt effect (PZSE). However,
4 100 this option is impossible to set in practice as for most HS materials the PZSE corresponds
5 101 to pH values much lower than 3, i.e. conditions where HS charge tends to 0 and HS are
6 102 prone to the formation of aggregates (especially so for the humic fraction).

7
8
9 103 (ii) The positioning of the different IS curves relatively to one another (hereafter referred to
10 104 as “relative curve positioning”) requires an additional independent salt titration at a
11 105 chosen fixed pH, commonly known as pH stat salt titration.³⁰ This option is not optimal
12 106 because of the additional measurement time it requires and the possible associated
13 107 uncertainties in the ensuing relative curve positioning process brought by the analysis of
14 108 a different sample.

15
16
17
18
19 109 Theoretical evaluation of HS charge properties from acid-base titration data is also highly
20 110 challenging. Substantial efforts have been made to estimate thermodynamic proton- and metal
21 111 ion-HS binding parameters and to develop predictive models under environmentally relevant
22 112 conditions.^{4,7,10,25,29,31–34} Historical models on protons binding by HS treat humic substances as
23 113 mixtures of dissolved aqueous solutes. Most of these models trace their origin to the Langmuir
24 114 equation. The Henderson-Hasselbalch equation, a linearized logarithmic version of the
25 115 Langmuir equation, can be represented using multiple Langmuir sites, which leads ultimately
26 116 to the Gaussian distribution model. The Freundlich model is an entirely empirical isotherm
27 117 allowing infinite binding in its unbounded original form; this model is nearly equivalent to a
28 118 Gaussian distribution of Langmuir binding sites in its bounded form, as mathematically proven
29 119 by Sips.³⁵ The well-known hybrid Langmuir-Freundlich model (whose linearized logarithmic
30 120 form is known as the modified Henderson-Hasselbalch equation), often involves two types of
31 121 sites to describe proton binding on HS and to fit experimental data for complex HS mixtures.
32 122 Other models like Models WHAM V or VI may integrate more binding sites (up to 8) and they
33 123 came as improvement to the aforementioned pioneering theoretical representations as they
34 124 included effects associated to electrostatics of HS viewed as particles and not as solutes. Indeed,
35 125 previous study³⁶ demonstrated that HS electrophoretic properties, in particular their dependence
36 126 on solution ionic strength, could be properly interpreted using electrohydrodynamic theory for
37 127 soft (ion-permeable) particles. The successful interpretation also applied to large ionic strengths
38 128 where historical electrokinetic models valid for solutes or molecules (e.g. Hückel-Onsager
39 129 formalism) failed in reproducing quantitatively the peculiar electrokinetic behavior of soft
40 130 particles under such electrolyte concentration conditions.^{37,38} As a further support for
41 131 representing HS materials as (nano)particles rather than solutes, we mention that the
42 132 chemodynamics of metal-humics or metal-fulvics complexes (which refers to the

1
2
3 133 interconversion kinetics between free and complexed metal forms) cannot be understood at a
4 134 quantitative level on the basis of the well-known Eigen metal complexation model that is strictly
5 135 applicable to ligands of small molecular size.³⁹ Instead, a kinetic model elaborated with a
6 136 nanoparticulate representation of humics with adequate electrostatics evaluated from Poisson-
7 Boltzmann theory for soft nanocolloids was shown to correctly capture the way kinetics of
8 137 metal association with humics and fulvics depends on particle size and electrostatic properties
9 138 as well as on the metal nature.³⁹ The remarkable dynamic reactivity of nanoparticulate humics
10 139 and fulvics originate from Boltzmann metal accumulation and Debye acceleration of metal
11 140 transport, most pronounced for soft particles that exploit accelerating mechanism on a 3D
12 141 level.³⁹ Last, we emphasize that measured diffusion coefficients of humics and fulvics, in the
13 142 range $2.5 \times 10^{-10} \text{ m}^2 \text{ s}^{-1}$ to $6.9 \times 10^{-11} \text{ m}^2 \text{ s}^{-1}$ for two of the samples analyzed here (i.e. Suwannee
14 143 River Natural Organic Matter and Pahokee Peat Humic Acid)⁴⁰ better fit a particle-based
15 144 representation for HS rather than a molecular/solute one. Typical diffusion coefficients for
16 145 molecules range indeed from $6.23 \times 10^{-10} \text{ m}^2 \text{ s}^{-1}$ (for citric acid $\sim 200 \text{ g mol}^{-1}$) to $4.14 \times 10^{-10} \text{ m}^2$
17 146 s^{-1} (for rhodamine 6G $\sim 500 \text{ g mol}^{-1}$).^{41,42}

18
19
20
21
22
23
24
25
26
27 148 Further benefits in adopting Poisson Boltzmann theory for HS particles were evidenced by
28 149 Pinheiro et al.¹⁷ in their analysis of potentiometric titration curves collected for a large variety
29 150 of HS. In detail, these authors reported a formalism called SPBT-PEST (SPBT for Soft Poisson
30 Boltzmann-based Titration theory and PEST as the module used for adjustment of SPBT-
31 151 parameters) to reconstruct experimental titration data on proton binding to HS with an analysis
32 152 based on rigorous numerical solving of non-linearized Poisson-Boltzmann equation for soft
33 153 nanoparticles. Practically, SPBT-PEST analysis of potentiometric titration data involves the
34 154 concomitant reconstruction of both the measured titration data and the associated proton affinity
35 155 spectra over the whole range of pH and salt concentration conditions tested. It is stressed that
36 156 the SPBT-PEST model, when applied to chemical conditions where there are no electrostatic
37 157 effects, identifies with the Henderson-Hasselbalch equation. Within adopted particle-based
38 158 representation of HS, the Langmuir-Freundlich or Henderson-Hasselbalch isotherm may be
39 159 applicable, albeit at a local level within the reactive body of the HS, and the binding properties
40 160 perceived at the scale of the particle and that of the particle dispersion must then be retrieved
41 161 from proper spatial integration, as detailed elsewhere.¹⁷

42 162
43 163 Given the aforementioned elements, WHAM model VI/VII involving simple solution to
44 164 the Poisson-Boltzmann (PB) equation valid for hard particles (i.e. impermeable to ions from
45 165 background electrolytes), is unsuitable for HS, as further argued by Town et al.⁴³ and Rotureau

1
2
3 166 et al.⁴⁴ in the context of equilibrium metal binding to HS. Whereas NICA-Donnan model
4 167 represents HS as permeable spheres, the electrostatic potential profile associated to Donnan
5 168 representation is oversimplified as it implies a potential that is *a priori* constant inside the
6 169 particle. However, this simplification may result in a misevaluation of the proton and metal ion-
7
8 170 HS binding parameters as variation of inner particle potential with position is operational in
9 171 small-sized particles like many HS for which radius is comparable to Debye length.^{19,43,44}
10
11 172 Furthermore, the Tipping models or NICA-Donnan model do not allow a quantitative
12 173 interpretation of metal stability constants and heterogeneity thereof as measured with
13 174 electroanalytical techniques in media differing with respect to ionic strength.^{19,43,44}

14
15
16
17 175 As a response to the major limitations and challenges identified above, we develop herein
18 176 a new experimental and theoretical procedure allowing for a consistent determination of acid-
19 177 base HS features. We show that the new experimental approach we propose leads to: (i) a
20 178 reduction of the overall measurement time by a factor ~ 3 , (ii) a decrease of effects related to
21 179 sample dilution, and (iii) an improved relative positioning of titration data curves collected on
22 180 a given sample at different electrolyte concentrations. The data treatment process involves the
23 181 direct subtraction of an experimental blank to measured sample, and a robust method - here
24 182 explicitly detailed - for the evaluation of the absolute charge Q from the relative charge variation
25 183 ΔQ measured with changing pH and salt concentration. This evaluation is achieved by
26 184 exploiting proton affinity spectra defined as the first derivative of the titration curve with respect
27 185 to pH (dQ/dpH), spectra that do not depend on Q_0 . The parameters describing the intrinsic
28 186 heterogeneity of HS reactive sites as well as the chemical and electrostatic HS components to
29 187 proton binding mechanism are then recovered by consistent reconstruction of both proton
30 188 affinity spectra and titration data using SPBT-PEST model.¹⁸ Our approach is illustrated with
31 189 measurements on several widely used HS standards provided by the International Humic
32 190 Substance Society (IHSS).^{25,26,45,46} To the best of our knowledge, no acid-base titration data has
33 191 ever been reported for the most recent samples commercialized by the IHSS. The obtained
34 192 results are compared with ones published on these IHSS samples collected at the same location
35 193 but ca. 30 years ago.²⁶

36 194
37 195
38
39
40
41
42
43
44
45
46
47
48
49
50

196 Materials and Methods

197 **Reagents.** All 7 HS samples analyzed in this work were purchased from IHSS, their
198 abbreviated names adopted in this study together with their reference number are indicated in
199 brackets: three samples from Suwannee River, one humic acid, one fulvic acid and one natural
200 organic matter (respectively SRFA, 3S101F; SRHA 3S101H and SRNOM 2R101N), two from
201 Pahokee Peat fulvic and humic acid (respectively PPFA, 2S103F and PPHA, 1S103H), and two
202 humic acid samples from Leonardite (LHA, 1S104H) and from Elliot Soil (ESHA, 4S102H).
203 Reagents needed for the titration were acquired from Sigma Aldrich, namely acid (HCl, 0.1 mol
204 L⁻¹), base (NaOH 0.1 mol L⁻¹) and background NaCl electrolyte. The pH-buffer solutions
205 required for electrode calibrations were ROTI®Calipure products (pH 4.00, 5.00, 7.00, 9.00,
206 10.00). All samples were prepared with Ultrapure Water provided through a Milli-Q
207 purification system.

209 **Instruments.** All pH measurements were performed by a Hamilton Fluxtrode pH electrode.
210 Mettler Toledo analytical balance (± 0.0001 g) was used to weigh all HS samples. Acid, base
211 and salt additions during titration and HS dispersion process were conducted with an automated
212 Metrohm titrator 809 Titrando, connected to a TIAMO v2.4 program that operates three
213 burettes. Regarding the burettes, two of them had a volume of 10 mL and one of 2 mL, and they
214 were respectively filled with 0.1 M HCl, 2 M NaCl and 0.1 M NaOH solutions. A TIAMO
215 script was written for the titration protocol and is available on request.

217 **Sample preparation.** Sample solutions were prepared by mixing 25 mg of HS material,
218 50 ml of 1 mM NaOH and 9 mM NaCl directly into the titration Teflon vessel. The resulting
219 sample concentration (i.e. 500 mg of NOM L⁻¹) adopted in this work and in other studies⁴⁷⁻⁴⁹ is
220 optimal for the detection of variation in HS charge with changing solution pH as it avoids e.g.
221 the addition of large volume of titrants with use of sufficiently high concentrations in acid and
222 base. Christl et al.⁵⁰ investigated the effects of humic and fulvic acid concentrations (1-1000
223 mg/L) and ionic strength on copper and lead binding, and found that corresponding metal-
224 binding isotherms measured at high and low humic matter concentration were similar.
225 Reversible aggregation-disaggregation of HS particles may occur and aggregation issue is more
226 significant for humic acids than for fulvic acids. Particle aggregation is further most important
227 at low pH and high ionic strength. As we change the ionic strength at high pH (see titration
228 protocol in the next section), thereby spending far less time at low pH condition, we expect that

1
2
3 229 this specific aggregation problem will be less severe with the new titration methodology
4 230 proposed here. Our HS disaggregation protocol is applied to ensure that the dissolution of the
5 231 solid material is complete and that there is no significant amount of aggregates in solution. We
6 232 emphasize that the experimental verification (via diffusion coefficient measurement by
7 233 Dynamic Light Scattering, DLS, or by voltammetry¹⁷) for the occurrence or not of HS particle
8 234 aggregation under the conditions used for the titration measurements is not an easy task as e.g.
9 235 DLS will be affected by multiple scattering at the HS concentration of interest and voltammetric
10 236 measurements by the absence of signal as all cadmium ions will be then strongly complexed.
11 237 The vessel was placed in an ultrasonic bath for 1 minute to disperse any possibly occurring
12 238 aggregates. It was then placed in a thermoregulated glass vessel at 25°C under argon
13 239 atmosphere, and the solution was magnetically stirred during the entire titration experiment.
14 240 Subsequently, HS disaggregation protocol was initiated with a Titrand stand: HS solution was
15 241 first set at pH 10 using NaOH 0.1 M and the pH decrease was monitored during 1 hour. Then
16 242 the pH was set again to 10 and monitored overnight (usually 12 hours). Afterwards solution pH
17 243 was set at 3 using HCl 0.1M, just prior to application of the potentiometric titration protocol
18 244 detailed below.
19 245

20
21
22 246 **Potentiometric titration protocol.** Each sample titration was paired with a
23 247 corresponding blank titration performed either before or after sample titration. The hereafter-
24 248 described protocol applies to both the blank and the sample titration step. Five pH-buffer
25 249 solutions (pH = 4, 5, 7 and 9 and 10) were used to determine a pH-potential (E , in V) calibration
26 250 curve for the pH electrode prior and subsequent to a titration process (for both blank and sample
27 251 measurement). All titrations were conducted between pH 3 and 10.5 using potential control.
28 252 For each sample and associated blank measurement, titrations were successively conducted at
29 253 three solution ionic strengths: 10 mM, 30 mM and 100 mM NaCl. One of the main aspects of
30 254 the new experimental protocol is that the initial (E_{start}) and final (E_{end}) potential values - for all
31 255 three IS conditions in both blank and sample titrations - are rigorously kept equal to minimize
32 256 error in blank subtraction and curve positioning procedure.

33
34
35 257 After ensuring that E is stable for at least 15 mins and that it equals E_{start} (corresponding
36 258 to pH 3, IS =10 mM), the sample or blank solution was titrated with a base solution, with
37 259 increasing solution pH up to 10.5 (corresponding to E_{end}). Then, IS was increased from 10 mM
38 260 to 30 mM upon addition of 2 M NaCl solution. This led to a drift of E to a larger value (E_{drift}),
39 261 which was carefully monitored until it stabilized (within 15 min). After stabilization, E was set

again to E_{end} upon addition of a small volume of 0.1 M NaOH solution. The added amount was recorded and used later for relative curve positioning purpose. Subsequently, acid titration (using 0.1 M HCl) was performed to reach E_{start} . The entire procedure was repeated with: (i) a base titration up to E_{end} , (ii) an increase in IS to 100 mM NaCl concentration, (iii) a careful monitoring of E_{drift} , (iv) an addition of base to reach E_{end} again, and (v) a reverse and forward titration with acid and base, respectively.

We cautiously verified the correct electrode calibrations at the start and end of the titration experiments as these were found identical within experimental error, meaning that we did not observe any calibration drift in the course of the titration experiments.

The deprotonated groups carried by the HS (Q_{HS}) are determined by point-by-point subtraction of the blank titration for each pH condition tested^{51,52} (eq 1).

$$Q_{\text{HS}} = Q_{\text{HS+solution}} - Q_{\text{blank}} \quad (1)$$

where $Q_{\text{HS+solution}}$ and Q_{blank} represent the number of mols per liter of added titrant in the presence and absence of HS, respectively. This operation leads to estimation of Q_{HS} solely associated with HS titration with a reference of 0 moles L⁻¹ of charge at pH 3 and 10 mM salt concentration as the Q_0 value is unknown at this stage of the analysis. ΔQ (in mol kg⁻¹) was then calculated by dividing the blank-subtracted Q_{HS} value by the concentration of HS ([HS] in kg L⁻¹) (eq 2):

$$\Delta Q = \frac{Q_{\text{HS}}}{[\text{HS}]} \quad (2)$$

Fitting procedure. The SPBT-PEST fitting procedure applied to obtain the parameters that best describe the experimental titration curves and their associated proton affinity spectra closely follows the one proposed by Pinheiro et al.¹⁸ except for the very determination of Q_0 . This procedure is described in detail in section C of the Supporting Information (SI) of the paper by Pinheiro et al.¹⁸ the reader is referred to. The procedure consists in three steps that we briefly recall:

a) Initial parameter estimation

The input file needed to run SPBT-PEST model is a file containing the measured charge vs. pH and its associated proton affinity spectrum (dQ/dpH vs. pH). This affinity spectrum was obtained by cubic spline interpolation of the experimental Q vs. pH curve and evaluation of its derivative with respect to pH (step achieved using MatlabTM software). The required estimation of the particle radius (r_p , in m) and molecular weight (M_w , in kg mol⁻¹) is done along the lines detailed in the sections A and B of SI. Briefly, scanned stripping chronopotentiometry (SSCP) was used to determine r_p ⁵³ and values of M_w or realistic ranges thereof (minimum: $M_{w,\text{min}}$ to

1
2
3 295 maximum: $M_{w,max}$) were inferred from literature review. Guessed values for the density of
4 296 reactive carboxylic and phenolic groups (in mol kg⁻¹) were estimated from the experimental ΔQ
5
6 297 vs. pH curve, namely: carboxylic sites density ($Q_{max,1}$) was set equal to the value of ΔQ reached
7
8 298 at the first plateau encountered with increasing pH, density of phenolic groups ($Q_{max,2}$) was set
9
10 299 equal to the excess of measured charge relative to that plateau value. The initial guessed values
11
12 300 for the protonation (or dissociation) constants pertaining to carboxylic and phenolic groups
13
14 301 (pK_{a1} and pK_{a2} , respectively) were estimated from direct reading of the pH position of the
15
16 302 maxima in the proton affinity spectrum (dQ/dpH vs. pH). The parameters describing the
17
18 303 chemical heterogeneity of carboxylic and phenolic groups (m_1 and m_2 , respectively) were
19
20 304 initially set to 0.5 value according to the procedure described in section D of Pinheiro et al.¹⁸.
21
22 305 All values adopted for the initial guessed estimates of the relevant parameters listed above are
23
24 306 collected in Table S1 in SI (section C therein) for the IHSS samples of interest in this work.
25
26 307 They serve for initiating the iterative procedure detailed by Pinheiro et al.¹⁸ to recover the
27
28 308 measured proton titration data and associated proton affinity spectra.

29
30
31
32
33
34
35
36
37
38
39
40
41
42
43
44
45
46
47
48
49 309 *b) Q_0 determination*

50
51 310 The novel determination of Q_0 proposed in this work involves the exploitation of the
52
53 311 proton affinity spectrum (dQ/dpH), which can be calculated from the measured pH-dependence
54
55 312 of the charge variation (ΔQ) as formulated by eqs. 3 and 4:

56
57
58
59
60
313
$$Q = \Delta Q + Q_0 \quad (3)$$

314
$$\frac{dQ}{dpH} = \frac{d\Delta Q}{dpH} \quad (4)$$

315 Concomitant fitting of the proton affinity spectra, derived from the data measured at the
316 three adopted IS values, provides a full set of estimated parameters (r_p , M_w , $Q_{max,1}$, $Q_{max,2}$, pK_{a1} ,
317 pK_{a2} , m_1 , m_2). These parameters were obtained by adjustment of data with SPBT-PEST
318 formalism, and they are -by construction- independent of any arbitrary choice made for Q_0 .
319 These parameters then serve to compute newly corrected Q vs. pH curves for all three IS where
320 the value of Q_0 corresponds to the lowest Q value, i.e. at pH 3 and 10 mM NaCl.

321 *c) Refining the parameter values*

322 Refinement of the parameter values (r_p , M_w , $Q_{max,1}$, $Q_{max,2}$, pK_{a1} , pK_{a2} , m_1 , m_2) is
323 subsequently made from concomitant SPBT-PEST-based analysis of both Q and dQ/dpH
324 curves following steps 3a and 3b in section C of the SI of Pinheiro et al.¹⁸ The fitting procedure

1
2
3 325 is first applied by setting r_p and M_w to constant values while refining $Q_{\max,1}$, $Q_{\max,2}$, pK_{a1} , pK_{a2} ,
4 326 m_1 , m_2 , and then upon refining r_p and M_w whereas setting the other parameters constant.

5
6 327 It is stressed that adopted SPBT-PEST modeling is performed without including any
7
8 328 specific binding of Na^+ to HS, that is by regarding the background electrolyte medium as
9
10 329 indifferent with no role of the electrolyte ions in the processes that control the pristine structural
11 330 charge of the HS particles.¹⁷ This approximation, also made within NICA-Donnan based
12 331 modeling framework,²⁰ is legitimate due to the extremely weak binding of Na^+ to any ligand in
13
14 332 solution, as illustrated by its tendency to poorly hydrolyze (corresponding pK approximately
15
16 333 equal to 14).⁵⁴

17 334

20 335 Results and discussion

21
22 336 This section reports HS titration data measurements and theoretical treatment on the basis
23
24 337 of our proposed experimental protocol, namely blank subtraction, relative positioning of the
25
26 338 experimental titration curves at different IS and the absolute curve positioning once the charge
27
28 339 Q_0 at low pH is determined. Best fitted parameters from SPBT-PEST modeling of the data on
29 340 studied IHSS batches are given and compared with previously published results.

30 341

31
32 342 **Blank subtraction.** An example of blank, raw and blank-corrected sample titration curve
33
34 343 (Q_{exp} vs. pH) is given for Suwannee River Fulvic Acid (SRFA) at 10 mM NaCl in Figure 1. The
35
36 344 blank correction is classically conducted by theoretical interpolation of the experimental blank
37
38 345 titration curve and subsequent subtraction to sample titration data over the whole range of pH
39
40 346 values where they have been collected. Nevertheless, in addition to the exclusion of electrode
41
42 347 drift in the blank data fitting operation, the equation used for theoretical interpolation of blank
43
44 348 titration data poorly fits pH domains where steeped variations in material charge are measured.
45
46 349 These errors introduced during blank correction may, in turn, leads to erroneous “blank
47
48 350 corrected” curves of titrated sample. In order to compute a blank correction that integrates
49
50 351 electrode drift (if any) and truly represents experimental blank titration curve, the experimental
51
52 352 blank values were fitted by cubic spline function using Matlab™ software. This makes possible
53
54 353 the blank subtraction from sample titration data to be performed point by point.^{51,52} It is
55
56 354 emphasized that accurate experimental blank subtraction is possible if and only if blank and
57
58 355 sample titration curves start and end exactly at the same electrode potential (E_{start} and E_{end}
59
60 356 respectively), so as to minimize errors in pH domains where steep sloped sections are measured,
357
358
359
360 357 namely at low and high pH values. Last, additional smoothing of the cubic spline function

retrieved from blank titration data interpolation may be necessary in case of noisy blank titration data, recalling that specificity of cubic spline function is that it has to pass through all experimental data points subjected to interpolation.

As expected, resulting corrected titration curves obtained for all studied IHSS samples display a negative charge over the whole pH range studied, which is typical for natural organic matter.^{55–59}

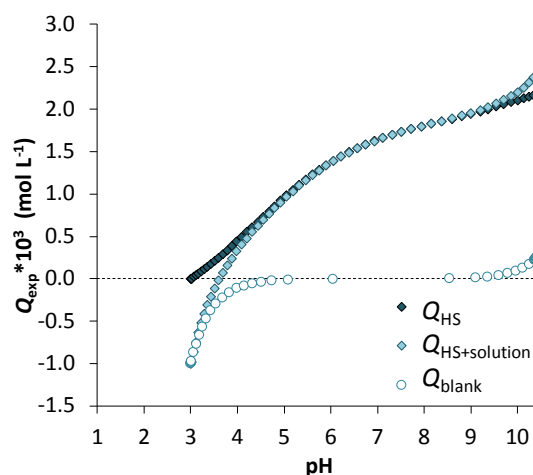


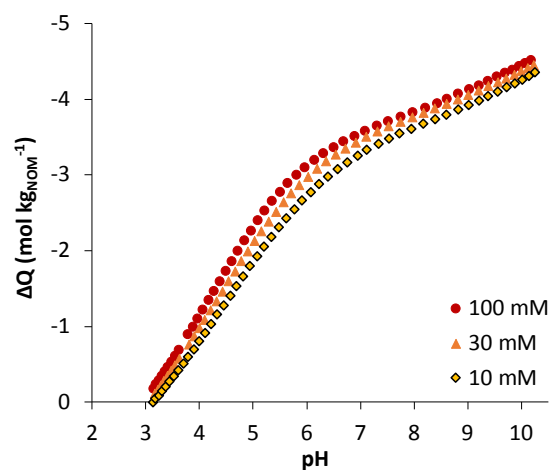
Figure 1: Experimental titration data versus pH. The Q_{HS} is computed from eq 1 determined at 10 mM background electrolyte solution for the blank solution (Q_{Blank}), the paired SRFA-containing solution ($Q_{HS+solution}$) and the difference between these data (Q_{HS}) are represented. The initial charge (pH 3) for the raw ($Q_{HS+solution}$) and blank (Q_{HS}) titration is given by the number of moles of acid anions $[Cl^-]$, and subsequent points are computed by adding the number of moles of cations of the titrant $[Na^+]$.

370 371 **Relative positioning of titration curves at different salt concentrations.**

372 Background electrolyte concentration affects proton-HS binding as it impacts the electrostatic
373 contribution to the overall interaction between HS and protons. As a direct consequence,
374 evaluation of this electrostatic component of HS reactivity towards protons critically depends
375 on the relative position of the titration curves measured at different solution ionic strengths. For
376 the sake of illustration, Figure S1 (section D in SI) shows a flawed relative positioning of
377 titration curves for SRFA “FH-03” sample given by Milne et al.²⁵ Unlike curves well positioned
378 with respect to electrolyte concentration (Figure S1), data (measured at 2, 10 and 100 mM
379 NaCl) by Milne et al.²⁵ display overlap over the entire range of pH values. As a consequence,
380 the interpretations derived from such titration curves presenting an overlap would imply that
381 the titrated HS material would have the same proton binding behavior regardless of solution
382 ionic strength IS, whereas opposite conclusion was extensively reported in literature.¹⁷ In Figure
383 2, titration curves of SRFA at three IS were positioned following the new procedure detailed in
384 the preceding section. According to our proposed methodology, salt addition is carried out at

1
2
3 385 the highest pH value when E_{end} is reached at the end of the base titration (step 1). Under such
4 386 conditions, HS charge and corresponding attractive electrostatic HS- H^+ interactions are
5 387 maximal.⁶⁰ This leads to a significant release of H^+ into the solution, which can be (i) accurately
6 388 monitored through pH-electrode ($E = E_{\text{drift}}$) as the charge variation exceeds electrode-
7 389 measurement error, and (ii) neutralized by precise addition of OH^- to reach E_{end} again (step 2).
8 390 The same procedure is carried out in the blank titration where the amount of OH^- necessary to
9 391 return to E_{end} is due to dilution effect. The difference of base number of moles, needed to return
10 392 to E_{end} , between sample and blank titration, represents the new HS charge resulting from
11 393 increase in salt concentration. To position the titration curves, the result of the equation 2 is
12 394 summed to the new HS charge after IS change.

13 395 This suggested approach cannot be implemented in the other commonly adopted
14 396 procedures where salt addition is made at the lowest pH value^{22,23} because E_{drift} is then not
15 397 measurable. The current approach offers the advantage to perform the entire titration procedure
16 398 in the same sample, without performing additional titration at fixed pH vs. salt concentration.³⁰
17 399 As a result, this procedure saves both time and lab work effort while eliminating possible
18 400 experimental biases.



401
402 **Figure 2:** Change in SRFA charge versus pH in comparison to the situation at pH 3 (ΔQ), as measured
403 at 10 mM, 30 mM and 100 mM NaCl.

404
405 **Fitting proton affinity spectra: absolute curve positioning by Q_0**
406 **determination.** ΔQ values provide limited information on HS acid-base properties. An
407 absolute positioning of the titration curves is required to fully address HS charge (Q). As
408 described in the experimental section, Q_0 is obtained via fitting the experimental proton affinity
409 spectra ($dQ/d(\text{pH})$) using SPBT-PEST iterative procedure. We recall that the initial guessed

1
2
3 410 estimates of the parameters involved in SPBT model (r_p , M_w , $Q_{\max,1}$, $Q_{\max,2}$, pK_{a1} , pK_{a2} , m_1 , m_2),
4 411 used to initiate the iterative computational process for reconstruction of proton affinity curves,
5 412 are listed in Table S1 for all HS materials analyzed in this work.

6
7 413 Theoretical reconstruction of the proton affinity spectra is illustrated in Figure 3a for
8 414 SRFA. Corresponding fitting provides a full set of newly adjusted SPBT parameters. These
9 415 adjusted parameters are then subsequently adopted to theoretically compute the charge curves
10 416 (Q) for each ionic strength tested. These theoretical curves are shifted to more negative charge
11 417 values (Figure 3b) as compared to measured ones simply because they account for the negative
12 418 electrical charge that HS material already carries under the starting conditions of the titration
13 419 measurement (i.e. pH = 3, 10 mM NaCl). Under such initial conditions, ΔQ was set to 0 as a
14 420 result of the blank subtraction. Accordingly, the value of the absolute charge Q_0 is directly
15 421 inferred from calculated Q at pH = 3 in 10 mM NaCl.

16 422 The Q_0 values (given in mol kg⁻¹) obtained for the different IHSS samples of interest in
17 423 this work (see the corresponding experimental and reconstructed proton titration curves in
18 424 Figure S2, section E in SI) were found to be larger for tested fulvic acids and NOM (SRFA -
19 425 1.00, PPFA -1.75, SRNOM -1.27) than for the humic acids (SRHA -0.69, PPHA -0.62, LHA -
20 426 0.70, ESHA -0.94), in line with the larger overall charge and acidity of fulvic acids known for
21 427 IHSS samples.²⁶ The developed method was applied to the most recently extracted and purified
22 428 IHSS samples (next section).

23
24
25
26
27
28
29
30
31
32
33 429
34
35
36
37
38
39
40
41
42
43
44
45
46
47
48
49
50
51
52
53
54
55
56
57
58
59
60

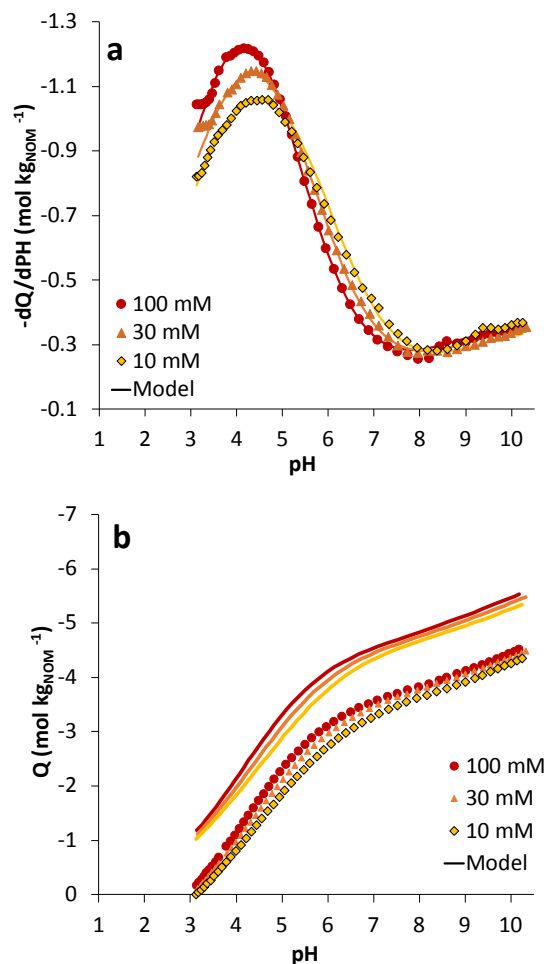


Figure 3: (a) Experimental and modeled proton affinity spectra for SRFA (dQ/dpH versus pH) at three IS (10 mM, 30 mM, 100 mM). (b) Experimental ΔQ (symbols) and simulated Q (lines) (versus pH and salt concentration) by SPBT-PEST for SRFA versus pH at three IS (10 mM, 30 mM, 100 mM). In both panels, experimental data are represented by symbols whereas modeled results are plotted by solid lines with the same color code as that for corresponding experimental data.

IHSS samples, thirty years after. The corrected proton titration curves established for the whole set of here studied HS materials are compared with those obtained for the first IHSS samples analyzed at 0.1 M ionic strength by Ritchie and Perdue²⁶, recalling that the latter samples were extracted and purified about 30 years ago. When comparing ΔQ plotted from both data sets (data acquired by Ritchie and Perdue²⁶ and data acquired in this study) at pH 3, a difference of less than 5% is obtained (Figure S3, section F in SI). This may suggest that the temporal variability of HS acid-base properties is rather small. A detailed comparison can be carried by recalculating the charge values published by Ritchie and perdue²⁶ at 0.1 M IS using modified Henderson-Hasselbalch model with optimized parameters (denoted as Q_1' , Q_2' , $\text{Log } k_1$, $\text{Log } k_2$, n_1 and n_2 in Ritchie and Perdue²⁶) and converting into mol kg⁻¹ of NOM from values

1
2
3 447 in meq gC⁻¹. We found that the experimental total HS charge is larger than that measured in this
4 448 work (Figure S4, section G in SI) due to a larger Q_0 determined by Ritchie and Perdue.²⁶ This
5
6 449 leads to different proportions of functional groups as exemplified for SRFA by the ca. 4 to 1
7
8 450 carboxylic to phenolic ratio reported by Ritchie and Perdue²⁶ as well as in other studies^{25,33}
9
10 451 which is higher than the 2 to 1 ratio obtained in the current study. This comparison emphasizes
11 452 how differences in computation of Q_0 (i.e. absolute positioning of titration curves) leads to
12 453 possible misevaluation of carboxylic sites density. We stress that HS charge evaluation in
13
14 454 Ritchie and Perdue²⁶ is based on an approach assuming that all carboxyl groups and no phenolic
15
16 455 groups are titrated at pH 8 and that one half of the phenolic groups are titrated between pH 8
17 456 and pH 10. We argue that our model fits all experimental data without such *a priori* assumption.
18
19 457 In addition, a prerequisite for the application of the Henderson-Hasselbalch equation adopted
20 458 in Ritchie and Perdue²⁶ (without any electrostatic component included) is that data subjected to
21 459 fitting using that equation must necessarily refer to a so-called master curve (i.e. all HS charges
22 460 are completely screened and there is no polyelectrolyte effect at stake). Obviously, any simple
23 461 look at the data cannot directly and quantitatively inform on the presence/absence of
24 462 electrostatic effects, and the hypothesis underlying a valid application of the Henderson-
25 463 Hasselbalch equation (without electrostatic component included) is -to the best of our
26 464 knowledge- rarely justified. By contrast, our approach combining HS charge evaluation at
27 465 different IS allows for refined and consistent consideration of HS electrostatics.
28
29
30
31
32
33
34

35 466
36 467 **SPBT parameters refinement.** Using the determined Q_0 values, all ΔQ titration data
37 468 could be converted into an absolute charge scale (Q). A refinement of the SPBT parameters
38 469 was then carried out by simultaneous fitting of both Q and dQ/dpH vs. pH curves¹⁸ using as
39 470 initial guessed parameter values those derived from SPBT-PEST-based fitting of the proton
40 471 affinity spectra. The refined parameters for the 7 here-examined samples (SRFA, SRHA,
41 472 SRNOM, PPFA, PPHA, LHA, ESHA) are collected in Table 1. The experimental and SPBT-
42 473 PEST modeled titration curves are all displayed in Figure 4 for SRFA, and in Figure S2 for the
43 474 other six IHSS samples. All modeled curves are in remarkable agreement with the measured
44 475 titration curves.

45 476 The fitted r_p values do not significantly differ from the measured ones for most of HS
46 477 samples, except for PPFA with $r_p = 1.56 \pm 0.34$ nm (measured) and 2.75 ± 0.14 nm (fitted value),
47 478 and PPHA with $r_p = 3.04 \pm 0.25$ nm (measured) and 3.67 ± 0.28 nm (fitted). As a possible
48 479 explanation for these deviations, it can be argued that SSCP used for the determination of r_p

1
2
3 480 (Section A in SI) is more sensitive towards smaller particles that diffuse faster.⁵³ Therefore, in
4 481 a polydisperse system this measurement may be biased by the presence of small particles,
5
6 482 possibly leading to an underestimation of the mean particle size of the sample.

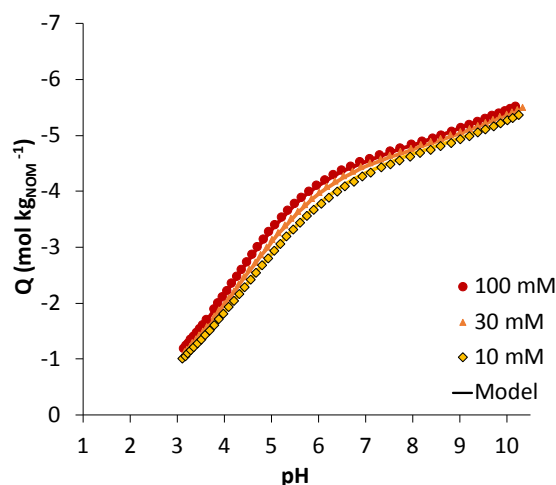
7
8 483 All fitted values of M_w fall within the intervals of measured values reported in literature
9
10 484 (Table S1). In detail, fitted values of M_w were close to $M_{w,\min}$ values given for SRFA, SRNOM,
11 485 PPFA, LHA and ESHA, whereas those of PPHA lie in the mid-range in the interval 6.4 to 19.2
12 486 kg mol⁻¹ with a fitted value of 11.10 kg mol⁻¹. For SRHA, $M_w = 4.02$ kg mol⁻¹ compares to
13 487 $M_{w,\max}$ (4.4 kg mol⁻¹).

14
15 488 The retrieved size and molecular weight seem to differ according to the respective
16 489 origins of the tested samples. The river-extracted samples indeed display - in average - smaller
17 490 r_p (ranging from 0.8 to 1.8 nm) and M_w (ranging from 1.14 to 4.02 kg mol⁻¹) than the peat and
18 491 soil ones ($1.71 < r_p < 3.67$ nm; $3.64 < M_w < 11.10$ kg mol⁻¹). Furthermore, some similarities can
19 492 be drawn between samples of the same nature, as humic particles samples are larger and heavier
20 493 than fulvic ones.⁶¹ These results are supported by other studies that associate larger and heavier
21 494 particles to terrestrial refractory molecules originating from plant residues, and smaller and
22 495 lighter particles associated to more labile particles such as bacterial-sourced organic matter.^{62,63}
23
24 496 No such cluster is observed regarding the $Q_{\max,i}$, $pK_{a,i}$ and m_i parameters (with $i = 1$ or 2). The
25 497 acidity constants are distributed from 3.29 to 4.33 and from 9.24 to 11.31 for carboxylic and
26 498 phenolic sites, respectively. Also, the heterogeneity parameters are in average 0.51 ± 0.068 and
27 499 0.28 ± 0.10 for carboxylic and phenolic sites, respectively.

28
29 500 The obtained density of carboxylic sites ranges from to 3.31 to 6.42 mol kg⁻¹, whereas
30 501 that of the phenolic sites lies in between 1.10 and 4.48 mol kg⁻¹. The carboxylic-to-phenolic
31 502 site density ratios ranges from 0.8 (for ESHA and PPHA) to 5.8 (for PPFA). Table S2 (section
32 503 H in SI) compares site densities ratios of carboxylic and phenolic groups in IHSS samples from
33 504 several studies^{26,25,64} with results obtained from this work. Although different data acquisition
34 505 and treatment methods were used in these various studies, they systematically report $Q_{\max,1} >$
35 506 $Q_{\max,2}$, in contrast to our findings. Most of the models describing titration curves used in the
36 507 studies with which our carboxylic-to-phenolic ratios are compared,^{25,26,64} do not explicitly
37 508 account for the electrostatic contribution to protons binding. Also, as mentioned in the
38 509 introduction section, there is no clear explanation as how Q_0 was determined in these studies.
39 510 For these reasons, we hypothesize that the carboxylic to phenolic ratio found therein might have
40 511 been misevaluated. Consequently, we argue that inaccuracy in determining Q_0 and in describing
41 512 the titration curves with unsuitable chemical-electrostatic model may have significant

513 implications for the estimation of parameters pertaining to the intrinsic chemical component of
 514 HS charge.

515



516
 517 **Figure 4:** Fully corrected experimental titration curves (symbols) and SPBT modelled titration curves
 518 (plain lines) for SRFA at 10 mM, 30 mM and 100 mM of NaCl.

519

520

521 **Table 1:** Optimized chemical parameters retrieved from SPBT-PEST modelling of titration data and
 522 associated proton affinity spectra.

| Sample | $Q_{\max,1}$ mol kg ⁻¹ | $Q_{\max,2}$ mol kg ⁻¹ | pKa ₁ | pKa ₂ | m_1 | m_2 | r_p (nm) | M_w kg mol ⁻¹ |
|--------|--------------------------------------|--------------------------------------|------------------|------------------|----------------|----------------|----------------|-------------------------------|
| SRFA | -4.35 ± 0.06 | -2.40 ± 0.30 | 3.76 ± 0.01 | 9.50 ± 0.28 | 0.57 ± 0.01 | 0.26 ± 0.03 | 1.34 ± 0.03 | 1.51 ± 0.06 |
| SRHA | -3.31 ± 0.15 | -3.87 ± 0.98 | 3.80 ± 0.02 | 10.04 ± 0.65 | 0.54 ± 0.02 | 0.24 ± 0.05 | 1.80 ± 0.03 | 4.02 ± 0.01 |
| SRNOM | -4.33 ± 0.05 | -3.38 ± 0.27 | 3.26 ± 0.01 | 9.73 ± 0.25 | 0.58 ± 0.01 | 0.24 ± 0.01 | 0.89 ± 0.04 | 1.15 ± 0.09 |
| PPFA | -6.42 ± 0.02 | -1.10 ± 0.05 | 3.66 ± 0.01 | 9.43 ± 0.09 | 0.40 ± 0.01 | 0.46 ± 0.02 | 2.75 ± 0.14 | 3.64 ± 1.09 |
| PPHA | -3.40 ± 0.26 | -4.26 ± 2.35 | 4.04 ± 0.02 | 11.31 ± 1.83 | 0.52 ± 0.03 | 0.20 ± 0.06 | 3.67 ± 0.28 | 11.10 ± 3.30 |
| LHA | -4.01 ± 0.13 | -2.00 ± 0.37 | 4.33 ± 0.05 | 9.24 ± 0.21 | 0.43 ± 0.01 | 0.41 ± 0.07 | 3.39 ± 0.37 | 5.78 ± 5.24 |
| ESHA | -3.74 ± 0.12 | -4.48 ± 1.34 | 3.27 ± 0.02 | 10.76 ± 1.06 | 0.51 ± 0.02 | 0.20 ± 0.02 | 1.71 ± 0.15 | 7.69 ± 3.21 |

523

524 Environmental implications

525 Potentiometric acid-base titration of nanoparticulate HS at different salt concentrations
 526 is a method of choice to determine HS charge properties. A proper interpretation of the
 527 corresponding data and ensuing evaluation of proton-HS binding is a mandatory pre-requisite
 528 for addressing at a mechanistic level the reactivity of HS with respect to e.g. metal ions or

1
2
3 529 mineral surfaces. Correctness in such data interpretation is tied to: (i) adequate positioning of
4 530 the raw proton titration curves measured at different salt concentrations and their correction for
5
6 531 blank titration, and (ii) appropriate deciphering of the intrinsic chemical and non-specific
7
8 532 electrostatic contributions to proton binding. The potentiometric acid-base titration protocol
9
10 533 developed in this work for characterizing HS charging behavior and the corresponding data
11
12 534 analysis methodology we propose overcome most of the so-far unresolved technical limitations
13
14 535 and biases that we herein identify. Our theoretical interpretative framework further solves the
15
16 536 inherent shortcomings of conventional thermodynamic models largely used for the analysis of
17
18 537 proton titration HS data but unfortunately based on an flawed representation of the electrostatics
19
20 538 operational for soft nano-HS particles.

21 539 Significant discrepancies are evidenced from comparison between proton titration
22
23 540 datasets established in this study for a large range of newly analyzed IHSS substances, and
24
25 541 those available in literature for similar samples. Outcome thus pinpoints possible flawed
26
27 542 experimental setup and/or unclear or even inappropriate data treatment methods adopted in the
28
29 543 past. A major point of concern is that these literature data have been extensively used to
30
31 544 calibrate empirical and phenomenological models for ‘predicting’ HS reactivity, putting aside
32
33 545 the large limitations of these models in their account of the true potential distribution in the
34
35 546 intra- and extra-particulate HS spatial regions. As a result, reactive HS site densities and
36
37 547 especially dissociation constants of carboxylic and phenolic HS functional groups reported in
38
39 548 literature are likely subjected to some uncertainties. In turn, predictions of HS reactivity towards
40
41 549 protons or even metal species as reported on the basis of such biased experimental titration data
42
43 550 and analysis thereof should be considered with caution. For the sake of illustration, whereas
44
45 551 carboxylic sites are generally considered to be more abundant than phenolic groups, the results
46
47 552 detailed in this work add much nuance to this accepted property, depending on the type of
48
49 553 considered HS material. When comparing the *relative* HS charge variation (relative to HS
50
51 554 charge at pH 3) at 0.1M solution ionic strength, we observe small differences (less than 5%)
52
53 555 between acid-base properties of 7 HS samples newly provided by the IHSS and those derived
54
55 556 from data collected on equivalent samples extracted 30 years ago. Because these HS samples
56
57 557 largely serve as reference to investigate NOM reactivity towards metal ions, a re-evaluation of
58
59 558 cations-HS binding data and modeling may be achieved with improved consideration of the
60
61 559 electrostatic component of protons binding and with caution to relative and absolute curves
62
63 560 positioning, as done in this work.

64 561 By analyzing 7 IHSS samples, a notable variability in proton-HS affinity is evaluated.
65
66 562 As previously reported, humic or fulvic samples show similarities, especially with respect to

1
2
3 563 their size and molecular weight, which was a major argument for past establishment of generic
4 564 parameters for popular HS reactivity models. However, HS from aquatic and terrestrial origins
5 565 define two types of HS and HA/FA grouping with respect to their overall charge behavior. In
6 566 line with previous criticisms formulated on empirical NICA-Donnan modeling, we recommend
7 567 to perform potentiometric acid-base titration and we advocate for the derivation of specific
8 568 interpretation of data collected on samples of interest rather than resort to the use of generic
9 569 parameters. This work provides reliable tools and fast methodological strategy to achieve these
10 570 required tasks and to better understand HS reactivity to metal ions or mineral surfaces, as
11 571 required in the analysis of numerous major environmental issues.

12 572 **Acknowledgments**

13
14
15
16 573 This work was supported by the C-FACTOR project funded by ANR (project number ANR-
17 574 18-CE01-0008; coordinator: R. Marsac). This work was carried out in the Pôle de compétences
18 575 Physico-Chimie de l'Environnement, LIEC laboratory UMR 7360 CNRS - Université de
19 576 Lorraine.
20
21
22
23
24
25
26
27
28
29
30
31
32
33
34
35
36
37
38
39
40
41
42
43
44
45
46
47
48
49
50
51
52
53
54
55
56
57
58
59
60

577 **References**

- 578 (1) Berner, R. A. Jacques-Joseph Ébelmen, the Founder of Earth System Science. *Comptes Rendus*
579 *Geosci.* **2012**, *344* (11–12), 544–548. <https://doi.org/10.1016/j.crte.2012.08.001>.
- 580 (2) Prentice, I. C.; Farquhar, G. D.; Fasham, M. J. R.; Goulden, M. L.; Heimann, M.; Jaramillo, V.
581 J.; Kheshgi, H. S.; LeQuéré, C.; Scholes, R. J.; Wallace, D. W. R. The Carbon Cycle and
582 Atmospheric Carbon Dioxide. In *Climate Change 2001: the Scientific Basis. Contributions of*
583 *Working Group I to the Third Assessment Report of the Intergovernmental Panel on Climate*
584 *Change*; Houghton, J. T., Ding, Y., Griggs, D. J., Noguer, M., van der Linden, P. J., Dai, X.,
585 Maskell, K., Johnson, C. A., Eds.; Cambridge University Press: Cambridge, UK, 2001; pp 185–
586 237.
- 587 (3) Raich, J. W.; Potter, C. S. Global Patterns of Carbon Dioxide Emissions from Soils. *Glob.*
588 *Biogeochem. Cycles* **1995**, *9* (1), 23–36. <https://doi.org/10.1029/94GB02723>.
- 589 (4) Kinniburgh, D. G.; van Riemsdijk, W. H.; Koopal, L. K.; Borkovec, M.; Benedetti, M. F.; Avena,
590 M. J. Ion Binding to Natural Organic Matter: Competition, Heterogeneity, Stoichiometry and
591 Thermodynamic Consistency. *Colloids Surf. Physicochem. Eng. Asp.* **1999**, *151* (1–2), 147–166.
592 [https://doi.org/10.1016/S0927-7757\(98\)00637-2](https://doi.org/10.1016/S0927-7757(98)00637-2).
- 593 (5) Buffle, J. Complexation Reactions in Aquatic Systems; Analytical Approach. *Acta Hydrochim.*
594 *Hydrobiol.* **1989**, *17* (2), 230–230. <https://doi.org/10.1002/ahch.19890170220>.
- 595 (6) Schnitzer, M. Effect of Low pH on the Chemical Structure and Reaction of Humic Substances.
596 In *Effects of Acid Precipitation on Terrestrial Ecosystems*; Hutchinson, T. C., Havas, M., Eds.;
597 Springer US: Boston, MA, 1980; pp 203–222. https://doi.org/10.1007/978-1-4613-3033-2_18.
- 598 (7) Benedetti, M. F.; Milne, C. J.; Kinniburgh, D. G.; Van Riemsdijk, W. H.; Koopal, L. K. Metal
599 Ion Binding to Humic Substances: Application of the Non-Ideal Competitive Adsorption Model.
600 *Environ. Sci. Technol.* **1995**, *29* (2), 446–457. <https://doi.org/10.1021/es00002a022>.
- 601 (8) Marang, L.; Eidner, S.; Kumke, M. U.; Benedetti, M. F.; Reiller, P. E. Spectroscopic
602 Characterization of the Competitive Binding of Eu(III), Ca(II), and Cu(II) to a Sedimentary
603 Originated Humic Acid. *Chem. Geol.* **2009**, *264* (1–4), 154–161.
604 <https://doi.org/10.1016/j.chemgeo.2009.03.003>.
- 605 (9) Marsac, R.; Catrouillet, C.; Davranche, M.; Bouhnik-Le Coz, M.; Briant, N.; Janot, N.; Otero-
606 Fariña, A.; Groenenberg, J. E.; Pédrot, M.; Dia, A. Modeling Rare Earth Elements Binding to
607 Humic Acids with Model VII. *Chem. Geol.* **2021**, *567*, 120099.
608 <https://doi.org/10.1016/j.chemgeo.2021.120099>.
- 609 (10) Milne, C. J.; Kinniburgh, D. G.; van Riemsdijk, W. H.; Tipping, E. Generic NICA–Donnan
610 Model Parameters for Metal-Ion Binding by Humic Substances. *Environ. Sci. Technol.* **2003**, *37*
611 (5), 958–971. <https://doi.org/10.1021/es0258879>.
- 612 (11) Pinheiro, J. P.; Mota, A. M.; Benedetti, M. F. Effect of Aluminum Competition on Lead and
613 Cadmium Binding to Humic Acids at Variable Ionic Strength. *Environ. Sci. Technol.* **2000**, *34*
614 (24), 5137–5143. <https://doi.org/10.1021/es0000899>.
- 615 (12) Tipping, E.; Rey-Castro, C.; Bryan, S. E.; Hamilton-Taylor, J. Al(III) and Fe(III) Binding by
616 Humic Substances in Freshwaters, and Implications for Trace Metal Speciation. *Geochim.*
617 *Cosmochim. Acta* **2002**, *66* (18), 3211–3224. [https://doi.org/10.1016/S0016-7037\(02\)00930-4](https://doi.org/10.1016/S0016-7037(02)00930-4).
- 618 (13) Marsac, R.; Banik, N. L.; Lützenkirchen, J.; Catrouillet, C.; Marquardt, C. M.; Johannesson, K.
619 H. Modeling Metal Ion-Humic Substances Complexation in Highly Saline Conditions. *Appl.*
620 *Geochem.* **2017**, *79*, 52–64. <https://doi.org/10.1016/j.apgeochem.2017.02.004>.
- 621 (14) Thurman, E. M.; Wershaw, R. L.; Malcolm, R. L.; Pinckney, D. J. Molecular Size of Aquatic
622 Humic Substances. *Org. Geochem.* **1982**, *4* (1), 27–35. [https://doi.org/10.1016/0146-6380\(82\)90005-5](https://doi.org/10.1016/0146-6380(82)90005-5).
- 623 (15) Slaveykova, V. I.; Wilkinson, K. J. Predicting the Bioavailability of Metals and Metal
624 Complexes: Critical Review of the Biotic Ligand Model. *Environ. Chem.* **2005**, *2* (1), 9–24.
625 <https://doi.org/10.1071/EN04076>.
- 626 (16) Van Leeuwen, H. P. Metal Speciation Dynamics and Bioavailability: Inert and Labile
627 Complexes. *Environ. Sci. Technol.* **1999**, *33* (21), 3743–3748.
628 <https://doi.org/10.1021/es990362a>.

- 1
2
3 630 (17) Van Leeuwen, H. P.; Duval, J. F. L.; Paulo Pinheiro, J.; Blust, R.; M. Town, R. Chemodynamics
4 631 and Bioavailability of Metal Ion Complexes with Nanoparticles in Aqueous Media. *Environ. Sci.*
5 632 *Nano* **2017**, *4* (11), 2108–2133. <https://doi.org/10.1039/C7EN00625J>.
- 6 633 (18) Pinheiro, J. P.; Rotureau, E.; Duval, J. F. L. Addressing the Electrostatic Component of Protons
7 634 Binding to Aquatic Nanoparticles Beyond the Non-Ideal Competitive Adsorption (NICA)-
8 635 Donnan Level: Theory and Application to Analysis of Proton Titration Data for Humic Matter.
9 636 *J. Colloid Interface Sci.* **2021**, *583*, 642–651. <https://doi.org/10.1016/j.jcis.2020.09.059>.
- 10 637 (19) Town, R. M.; van Leeuwen, H. P.; Duval, J. F. L. Rigorous Physicochemical Framework for
11 638 Metal Ion Binding by Aqueous Nanoparticulate Humic Substances: Implications for Speciation
12 639 Modeling by the NICA-Donnan and WHAM Codes. *Environ. Sci. Technol.* **2019**, *53* (15), 8516–
13 640 8532. <https://doi.org/10.1021/acs.est.9b00624>.
- 14 641 (20) Tipping, E.; Lofts, S.; Sonke, J. E. Humic Ion-Binding Model VII: A Revised Parameterisation
15 642 of Cation-Binding by Humic Substances. *Environ. Chem.* **2011**, *8* (3), 225.
16 643 <https://doi.org/10.1071/EN11016>.
- 17 644 (21) Koopal, L. K.; Saito, T.; Pinheiro, J. P.; Riemsdijk, W. H. van. Ion Binding to Natural Organic
18 645 Matter: General Considerations and the NICA–Donnan Model. *Colloids Surf. Physicochem. Eng.*
19 646 *Asp.* **2005**, *265* (1–3), 40–54. <https://doi.org/10.1016/j.colsurfa.2004.11.050>.
- 20 647 (22) Benedetti, M. F.; Van Riemsdijk, W. H.; Koopal, L. K. Humic Substances Considered as a
21 648 Heterogeneous Donnan Gel Phase. *Environ. Sci. Technol.* **1996**, *30* (6), 1805–1813.
22 649 <https://doi.org/10.1021/es950012y>.
- 23 650 (23) Nederlof, M. M.; De Wit, J. C. M.; Van Riemsdijk, W. H.; Koopal, L. K. Determination of Proton
24 651 Affinity Distributions for Humic Substances. *Environ. Sci. Technol.* **1993**, *27* (5), 846–856.
25 652 <https://doi.org/10.1021/es00042a006>.
- 26 653 (24) Ephraim, James.; Alegret, Salvador.; Mathuthu, Andrew.; Bicking, Margaret.; Malcolm, R. L.;
27 654 Marinsky, J. A. A Unified Physicochemical Description of the Protonation and Metal Ion
28 655 Complexation Equilibria of Natural Organic Acids (Humic and Fulvic Acids). 2. Influence of
29 656 Polyelectrolyte Properties and Functional Group Heterogeneity on the Protonation Equilibria of
30 657 Fulvic Acid. *Environ. Sci. Technol.* **1986**, *20* (4), 354–366. <https://doi.org/10.1021/es00146a007>.
- 31 658 (25) Milne, C. J.; Kinniburgh, D. G.; Tipping, E. Generic NICA-Donnan Model Parameters for Proton
32 659 Binding by Humic Substances. *Environ. Sci. Technol.* **2001**, *35* (10), 2049–2059.
33 660 <https://doi.org/10.1021/es000123j>.
- 34 661 (26) Ritchie, J. D.; Perdue, E. M. Proton-Binding Study of Standard and Reference Fulvic Acids,
35 662 Humic Acids, and Natural Organic Matter. *Geochim. Cosmochim. Acta* **2003**, *67* (1), 85–96.
36 663 [https://doi.org/10.1016/S0016-7037\(02\)01044-X](https://doi.org/10.1016/S0016-7037(02)01044-X).
- 37 664 (27) Vermeer, A. W. P.; van Riemsdijk, W. H.; Koopal, L. K. Adsorption of Humic Acid to Mineral
38 665 Particles. 1. Specific and Electrostatic Interactions. *Langmuir* **1998**, *14* (10), 2810–2819.
39 666 <https://doi.org/10.1021/la970624r>.
- 40 667 (28) Lenoir, T.; Matynia, A.; Manceau, A. Convergence-Optimized Procedure for Applying the
41 668 NICA-Donnan Model to Potentiometric Titrations of Humic Substances. *Environ. Sci. Technol.*
42 669 **2010**, *44* (16), 6221–6227. <https://doi.org/10.1021/es1015313>.
- 43 670 (29) Brassard, P.; Kramer, J. R.; Collins, P. V. Binding Site Analysis Using Linear Programming.
44 671 *Environ. Sci. Technol.* **1990**, *24* (2), 195–201. <https://doi.org/10.1021/es00072a006>.
- 45 672 (30) Tan, W. F.; Koopal, L. K.; Weng, L. P.; van Riemsdijk, W. H.; Norde, W. Humic Acid Protein
46 673 Complexation. *Geochim. Cosmochim. Acta* **2008**, *72* (8), 2090–2099.
47 674 <https://doi.org/10.1016/j.gca.2008.02.009>.
- 48 675 (31) Driver, S. J.; Perdue, E. M. Acidic Functional Groups of Suwannee River Natural Organic
49 676 Matter, Humic Acids, and Fulvic Acids. In *ACS Symposium Series*; Rosario-Ortiz, F., Ed.;
50 677 American Chemical Society: Washington, DC, 2014; Vol. 1160, pp 75–86.
51 678 <https://doi.org/10.1021/bk-2014-1160.ch004>.
- 52 679 (32) Sasaki, T.; Kobayashi, T.; Takagi, I.; Moriyama, H. Discrete Fragment Model for Complex
53 680 Formation of Europium(III) with Humic Acid. *J. Nucl. Sci. Technol.* **2008**, *45* (8), 718–724.
54 681 <https://doi.org/10.1080/18811248.2008.9711472>.
- 55 682 (33) Tipping, E. Humic Ion-Binding Model VI: An Improved Description of the Interactions of
56 683 Protons and Metal Ions with Humic Substances. *Aquat. Geochem.* **1998**, *4* (1), 3–47.
57 684 <https://doi.org/10.1023/A:1009627214459>.

- 1
2
3 685 (34) Chen, W.; Guéguen, C.; Smith, D. S.; Galceran, J.; Puy, J.; Companys, E. Comparing a Fully
4 686 Optimized ContinUouS (FOCUS) Method with the Analytical Inversion of Non Ideal
5 687 Competitive Adsorption (NICA) for Determining the Conditional Affinity Spectrum (CAS) of H
6 688 and Pb Binding to Natural Organic Matter. *Colloids Surf. Physicochem. Eng. Asp.* **2022**, *633*,
7 689 127785. <https://doi.org/10.1016/j.colsurfa.2021.127785>.
- 8 690 (35) Sips, R. On the Structure of a Catalyst Surface. *J. Chem. Phys.* **1948**, *16* (5), 490.
9 691 <https://doi.org/10.1063/1.1746922>.
- 10 692 (36) Duval, J. F. L.; Wilkinson, K. J.; van Leeuwen, H. P.; Buffle, J. Humic Substances Are Soft and
11 693 Permeable: Evidence from Their Electrophoretic Mobilities †. *Environ. Sci. Technol.* **2005**, *39*
12 694 (17), 6435–6445. <https://doi.org/10.1021/es050082x>.
- 13 695 (37) Duval, J. F. L.; Ohshima, H. Electrophoresis of Diffuse Soft Particles. *Langmuir* **2006**, *22* (8),
14 696 3533–3546. <https://doi.org/10.1021/la0528293>.
- 15 697 (38) Maurya, S. K.; Gopmandal, P. P.; Ohshima, H.; Duval, J. F. L. Electrophoresis of Composite
16 698 Soft Particles with Differentiated Core and Shell Permeabilities to Ions and Fluid Flow. *J. Colloid*
17 699 *Interface Sci.* **2020**, *558*, 280–290. <https://doi.org/10.1016/j.jcis.2019.09.118>.
- 18 700 (39) van Leeuwen, H. P.; Buffle, J.; Duval, J. F. L.; Town, R. M. Understanding the Extraordinary
19 701 Ionic Reactivity of Aqueous Nanoparticles. *Langmuir* **2013**, *29* (33), 10297–10302.
20 702 <https://doi.org/10.1021/la401955x>.
- 21 703 (40) Hosse, M.; Wilkinson, K. J. Determination of Electrophoretic Mobilities and Hydrodynamic
22 704 Radii of Three Humic Substances as a Function of PH and Ionic Strength. *Environ. Sci. Technol.*
23 705 **2001**, *35* (21), 4301–4306. <https://doi.org/10.1021/es010038r>.
- 24 706 (41) Petrášek, Z.; Schwille, P. Precise Measurement of Diffusion Coefficients Using Scanning
25 707 Fluorescence Correlation Spectroscopy. *Biophys. J.* **2008**, *94* (4), 1437–1448.
26 708 <https://doi.org/10.1529/biophysj.107.108811>.
- 27 709 (42) Vanýsek, P. *CRC Handbook of Chemistry and Physics*, Boca Raton.; CRC Press, 1992.
- 28 710 (43) Town, R. M.; Duval, J. F. L.; van Leeuwen, H. P. The Intrinsic Stability of Metal Ion Complexes
29 711 with Nanoparticulate Fulvic Acids. *Environ. Sci. Technol.* **2018**, *acs.est.8b02896*.
30 712 <https://doi.org/10.1021/acs.est.8b02896>.
- 31 713 (44) Rotureau, E.; Pinheiro, J. P.; Duval, J. F. L. On the Evaluation of the Intrinsic Stability of Indium-
32 714 Nanoparticulate Organic Matter Complexes. *Colloids Surf. Physicochem. Eng. Asp.* **2022**, *645*,
33 715 128859. <https://doi.org/10.1016/j.colsurfa.2022.128859>.
- 34 716 (45) Alberts, J. J.; Takács, M. Total Luminescence Spectra of IHSS Standard and Reference Fulvic
35 717 Acids, Humic Acids and Natural Organic Matter: Comparison of Aquatic and Terrestrial Source
36 718 Terms. *Org. Geochem.* **2004**, *35* (3), 243–256.
37 719 <https://doi.org/10.1016/j.orggeochem.2003.11.007>.
- 38 720 (46) Mobed, J. J.; Hemmingsen, S. L.; Autry, J. L.; McGown, L. B. Fluorescence Characterization of
39 721 IHSS Humic Substances: Total Luminescence Spectra with Absorbance Correction. *Environ.*
40 722 *Sci. Technol.* **1996**, *30* (10), 3061–3065. <https://doi.org/10.1021/es960132l>.
- 41 723 (47) Janot, N.; Reiller, P. E.; Korshin, G. V.; Benedetti, M. F. Using Spectrophotometric Titrations
42 724 To Characterize Humic Acid Reactivity at Environmental Concentrations. *Environ. Sci. Technol.*
43 725 **2010**, *44* (17), 6782–6788. <https://doi.org/10.1021/es1012142>.
- 44 726 (48) Cabaniss, S. E. Carboxylic Acid Content of a Fulvic Acid Determined by Potentiometry and
45 727 Aqueous Fourier Transform Infrared Spectrometry. *Anal. Chim. Acta* **1991**, *255* (1), 23–30.
46 728 [https://doi.org/10.1016/0003-2670\(91\)85082-4](https://doi.org/10.1016/0003-2670(91)85082-4).
- 47 729 (49) Christensen, J. B.; Tipping, E.; Kinniburgh, D. G.; Grøn, C.; Christensen, T. H. Proton Binding
48 730 by Groundwater Fulvic Acids of Different Age, Origins, and Structure Modeled with the Model
49 731 V and NICA–Donnan Model. *Environ. Sci. Technol.* **1998**, *32* (21), 3346–3355.
50 732 <https://doi.org/10.1021/es971134o>.
- 51 733 (50) Christl, I.; Metzger, A.; Heidmann, I.; Kretzschmar, R. Effect of Humic and Fulvic Acid
52 734 Concentrations and Ionic Strength on Copper and Lead Binding. *Environ. Sci. Technol.* **2005**, *39*
53 735 (14), 5319–5326. <https://doi.org/10.1021/es050018f>.
- 54 736 (51) Perdue, E. M.; Reuter, J. H.; Ghosal, M. The Operational Nature of Acidic Functional Group
55 737 Analyses and Its Impact on Mathematical Descriptions of Acid-Base Equilibria in Humic
56 738 Substances. *Geochim. Cosmochim. Acta* **1980**, *44* (11), 1841–1851.
57 739 [https://doi.org/10.1016/0016-7037\(80\)90233-1](https://doi.org/10.1016/0016-7037(80)90233-1).

- 1
2
3 740 (52) Sposito, G.; Holtzclaw, K. M. Titration Studies on the Polynuclear, Polyacidic Nature of Fulvic
4 741 Acid Extracted from Sewage Sludge-Soil Mixtures. *Soil Sci. Soc. Am. J.* **1977**, *41* (2), 330–336.
5 742 <https://doi.org/10.2136/sssaj1977.03615995004100020031x>.
- 6 743 (53) Pinheiro, J. P.; Domingos, R.; Lopez, R.; Brayner, R.; Fiévet, F.; Wilkinson, K. Determination
7 744 of Diffusion Coefficients of Nanoparticles and Humic Substances Using Scanning Stripping
8 745 Chronopotentiometry (SSCP). *Colloids Surf. Physicochem. Eng. Asp.* **2007**, *295* (1–3), 200–208.
9 746 <https://doi.org/10.1016/j.colsurfa.2006.08.054>.
- 10 747 (54) Baes, C. F.; Mesmer, R. S. The Hydrolysis of Cations. *Berichte Bunsenges. Für Phys. Chem.*
11 748 **1977**, *81* (2), 245–246. <https://doi.org/10.1002/bbpc.19770810252>.
- 12 749 (55) Neihof, R. A.; Loeb, G. I. The Surface Charge of Particulate Matter in Seawater. *Limnol.*
13 750 *Oceanogr.* **1972**, *17* (1), 7–16. <https://doi.org/10.4319/lo.1972.17.1.0007>.
- 14 751 (56) Neihof, R. Dissolved Organic Matter in Seawater and the Electric Charge of Immersed Surfaces'.
15 752 *J. Mar. Res.* **1974**, *32*, 5–12.
- 16 753 (57) Hunter, K. a. Microelectrophoretic Properties of Natural Surface-Active Organic Matter in
17 754 Coastal Seawater. *Limnol. Oceanogr.* **1980**, *25* (5), 807–822.
18 755 <https://doi.org/10.4319/lo.1980.25.5.0807>.
- 19 756 (58) Gerritsen, J.; Bradley, S. W. Electrophoretic Mobility of Natural Particles and Cultured
20 757 Organisms in Freshwaters1. *Limnol. Oceanogr.* **1987**, *32* (5), 1049–1058.
21 758 <https://doi.org/10.4319/lo.1987.32.5.1049>.
- 22 759 (59) Beckett, R.; Le, N. P. The Role or Organic Matter and Ionic Composition in Determining the
23 760 Surface Charge of Suspended Particles in Natural Waters. *Colloids Surf.* **1990**, *44*, 35–49.
24 761 [https://doi.org/10.1016/0166-6622\(90\)80185-7](https://doi.org/10.1016/0166-6622(90)80185-7).
- 25 762 (60) Ramos, A.; López, S.; López, R.; Fiol, S.; Arce, F.; Antelo, J. M. Effect of the Ionic Strength on
26 763 the Acid-Base Titration Curves of a Soil Fulvic Acid. *Analisis* **1999**, *27* (5), 414–417.
27 764 <https://doi.org/10.1051/analisis:1999270414>.
- 28 765 (61) Weng; Van Riemsdijk, W. H.; Koopal, L. K.; Hiemstra, T. Adsorption of Humic Substances on
29 766 Goethite: Comparison between Humic Acids and Fulvic Acids. *Environ. Sci. Technol.* **2006**, *40*
30 767 (24), 7494–7500. <https://doi.org/10.1021/es060777d>.
- 31 768 (62) Guggenberger, G.; Zech, W.; Haumaier, L.; Christensen, B. T. Land-Use Effects on the
32 769 Composition of Organic Matter in Particle-Size Separates of Soils: II. CPMAS and Solution ¹³C
33 770 NMR Analysis. *Eur. J. Soil Sci.* **1995**, *46* (1), 147–158. <https://doi.org/10.1111/j.1365-2389.1995.tb01821.x>.
- 34 771 (63) Machado, W.; Franchini, J. C.; de Fátima Guimarães, M.; Filho, J. T. Spectroscopic
35 772 Characterization of Humic and Fulvic Acids in Soil Aggregates, Brazil. *Heliyon* **2020**, *6* (6),
36 773 e04078. <https://doi.org/10.1016/j.heliyon.2020.e04078>.
- 37 774 (64) Fernandes, A. N.; Giacomelli, C.; Giovanella, M.; Vaz, D. O.; Szpoganicz, B.; Sierra, M. M. D.
38 775 Potentiometric Acidity Determination in Humic Substances Influenced by Different Analytical
39 776 Procedures. *J. Braz. Chem. Soc.* **2009**, *20* (9), 1715–1723. <https://doi.org/10.1590/S0103-50532009000900021>.
40 777
41 778
42 779